ELSEVIER

Biochimica et Biophysica Acta 1421 (1999) 39–52

BIOCHIMICA ET BIOPHYSICA ACTA
BBA

www.elsevier.com/locate/bba

Highly efficient immobilisation of antibody fragments to functionalised lipid monolayers

Inger Vikholm [a,*], Tapani Viitala [b,1], Willem M. Albers [a], Jouko Peltonen [b]

[a] *VTT Chemical Technology, P.O. Box 14021, FIN-33101 Tampere, Finland*
[b] *Department of Physical Chemistry, Åbo Akademi University, Porthansgatan 3–5, FIN-20500 Turku, Finland*

Received 12 April 1999; received in revised form 22 June 1999; accepted 28 June 1999

Abstract

The covalent attachment of Fab′ fragments of polyclonal anti-human IgG to a lipid with a terminal linker group was examined by means of quartz crystal microbalance and surface plasmon resonance measurements. The linker lipid was embedded in binary or ternary monolayers of dipalmitoylphosphatidylcholine (DPPC) and cholesterol. Atomic force microscopy images of the films deposited on silanised SiO_2 substrates showed that Fab′ fragments take a standing position, thus giving site-directed immobilisation. Human IgG forms a network on interaction with the antibodies. Non-specific binding of bovine serum albumin was found to be very low when DPPC was used as the host matrix. At an optimal Fab′ fragment concentration a binding capacity above 60% was obtained. However, if the surface concentration of the immobilised antibodies was too high, the binding capacity decreased due to steric hindrance. The results demonstrate that the covalent coupling of Fab′ fragments to *N*-(ε-maleimidocaproyl)-dipalmitoylphosphatidylethanolamine (DPPE-EMC) embedded in a host monolayer matrix of DPPC is a promising approach to achieve a site-directed immobilisation of antibodies with high antigen-binding efficiency.

Keywords: Antibody fragment; Phospholipid monolayer; Atomic force microscopy; Surface plasmon resonance; Quartz crystal microbalance; Antigen binding

1. Introduction

Surface plasmon resonance (SPR) and quartz crystal microbalance (QCM) measurements have been extensively used in the direct monitoring of biospecific interactions, particularly immunologic reactions [1–6]. The QCM is traditionally used to monitor and control the growth of thin films during vapour deposition and sputtering. The mass of the deposited film on the quartz crystal surface is indicated by the change of its resonance frequency [7]. In aqueous solutions, viscosity and elasticity effects of the layer and, moreover, embedded water contribute to the response [8–10]. The quartz crystal has been used for the first time in 1983 in immunologic measurements by Roederer and Bastiaans [2] and has been extensively used in academic studies as immunosensors [3] and also for monitoring the growth of biofilms [11]. SPR has been commonly applied to study molecular layers deposited on silver and gold surfaces [12], protein-binding to supported lipid membranes [13], interaction between antigens and antibodies [4–6] and between streptavidin and biotin

* Corresponding author.
[1] Also corresponding author. Present address: Graduate Schools of Materials Research, Turku, Finland.

0005-2736/99/$ – see front matter
PII: S0005-2736(99)00112-1

[14]. SPR is sensitive to changes in the refractive index and the thickness of the film on the metal surface.

Conventional immobilisation methods comprise adsorption of antibodies to polystyrene and covalent binding, e.g. to glass and silicon surfaces via the amino groups of the protein [15–17]. These methods are not site-directed and produce a random orientation of the antibody, which results in a very low binding efficiency. There are several options for site-directed immobilisation of antibodies. Antibodies can be attached through the saccharide moieties in their Fc part [18], to a specific site of the Fc region by protein A or protein G [16,17,19], or covalently attached through the free sulfhydryl group in the hinge region of Fab′ fragments [20–23]. Site-directed immobilisation has also been obtained by embedding lipid-tagged single chain antibodies into phospholipid monolayers [24]. Biotinylated antibodies have, furthermore, been coupled onto a surface by biotin/(strept)avidin chemistry [25]. Immobilisation of IgG via the Fc carbohydrate moieties has already been shown to produce higher binding efficiencies [26] and an improved sensor response [27] relative to the random immobilisation method via succinimide coupling to the amino groups of the protein.

Fab′ fragments have well-accessible reactive thiol groups opposite the antibody binding domains, which can be linked to different substrates with thiol-reactive reagents, containing maleimide or dithiopyridine. Ahluwalia et al. have attached Fab′ fragments to a monolayer of *N*,*N*-dioctadecyl-*N*-methyl-*N*-(2-mercaptoethyl) ammonium bromide [28]. Lu et al. have studied the immobilisation of anti-human IgG rabbit Fab′ fragments via γ-aminopropyltrimethoxy-silane on silica substrates and observed that the crosslinker *N*-succinimidyl-3-(2-pyridyldithio)-propionate gave a relatively larger immunological activity than the conventional glutardialdehyde immobilisation [29]. Jimbo and Saito have previously reported the immobilisation of Fab′ fragments onto plasma-polymerised layers via a maleimide [30].

Our approach has been to link Fab′ fragments to mixed monolayers of phospholipids. We have used the Langmuir–Blodgett (LB) technique to produce uniform and molecularly ordered lipid films on solid supports [31] and previously investigated the monolayer formation of two linker lipids in secondary and ternary systems of phosphatidylcholine and cholesterol [10,32]. Measurements with the QCM and radioimmunoassay demonstrated that Fab′ fragments could be coupled to a linker lipid embedded in a monolayer matrix of phosphatidylcholine with high antigen-binding efficiency [10,33].

In the present study, we have used atomic force microscopy (AFM) to image the layers in order to obtain information on the structural arrangement of the antibody fragments and the antigen, human IgG (hIgG). We have besides QCM and radioimmunoassay employed SPR to determine the binding efficiency. As SPR is sensitive to changes in the refractive index and the thickness of the film on the metal surface, these measurements provide an assessment of the immobilisation efficiency via a physicochemical parameter that is different from that of the QCM measurements.

2. Materials and methods

2.1. Lipids

The linker lipid DPPE-EMC was synthesised as previously described [10]. The linker lipid *N*-(ε-maleimidocaproyl)-dipalmitoylphosphatidylethanolamine (DPPE-EMC, Scheme 1) was prepared by the reaction of *N*-(ε-maleimidocaproyl)succinimide (EMCS, Fluka, purity >98%) with dipalmitoyl-*sn*-glycero-phosphatidylethanolamine (DPPE, Fluka, purity >99%) using triethylamine (Baker, purity >98%) as a homogeneous catalyst. The compound was purified by adsorption chromatography on silica gel 60.

The host matrix lipid 1,2-dipalmitoyl-*sn*-glycero-3-phosphatidylcholine, DPPC was purchased from Sigma (purity >99%), and cholesterol (CHOL) was from KSV Chemicals (Helsinki, Finland) (purity 99.8%).

2.2. Monolayer formation and deposition

The monolayers were prepared in a home made Teflon trough with dimensions of 50×200×10 mm using a commercial LB-instrument (KSV 2000, KSV Instruments, Helsinki, Finland). The lipids were dissolved in chloroform. DPPC was mixed with DPPE-EMC in a molar ratio of 9/1 and the molar ratio of

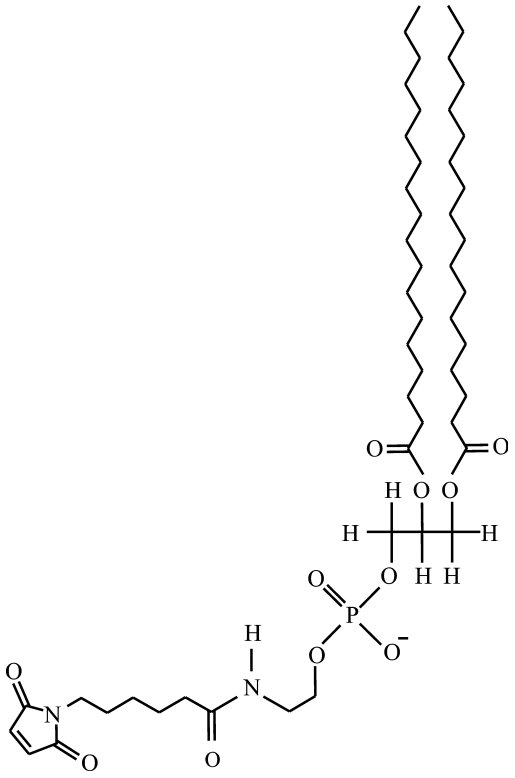

Scheme 1. Structure of the linker lipid DPPE-EMC.

DPPC/DPPE-EMC/CHOL was 4/1/5. The linker lipid matrices were spread onto an aqueous subphase of 10 mM HEPES, 150 mM NaCl, pH 6.8. High purity water (18.2 MΩcm) from a Milli-Q system (Millipore, Bedford, USA) was used for the preparation of the subphase and other buffer solutions. The monolayers were horizontally transferred at a surface pressure of 40 mN/m onto the solid substrates. The substrates were pressed into the subphase through the interface covered with the monolayer. The remaining lipids were removed from the interface and the substrates were rinsed with high-purity water and stored dry until further processing or analyses were performed.

The glass slides used for SPR measurements were coated with thin films of titanium (4 nm, to increase the adhesion of gold) and gold (37 nm) by vacuum evaporation. These substrates were then soaked in a 1 mM solution of octadecylmercaptan (ODM, Aldrich, purity 98%) in ethanol for 24 h, rinsed with ethanol and air dried before deposition (Au/ODM substrates). The silicon substrates used for RIA and AFM measurements (dimensions, 6×9 mm^2) were first peroxide treated to generate a maximum amount of silanol groups on the surface. The slides were then coated with octadecyltrichlorosilane (ODTCS, Aldrich, purity 95%) from toluene solutions, rinsed with toluene and air-dried before deposition (Si/ODTCS substrates).

2.3. Model antibodies

Human IgG (hIgG) and polyclonal goat anti-human F(ab′)$_2$ (from Jackson ImmunoResearch) was used as the model system. F(ab′)$_2$ was split into Fab′ fragments with dithiotreitol (DTT, Merck) typically under argon overnight in a microdialysis tube prior to use [34]. A value of 47 kDa was used for the molecular weight of Fab′ fragments [32].

2.4. Atomic force microscopy

The samples for AFM imaging were prepared in the following way: After the monolayers containing the linker lipids were transferred onto the Si/ODTCS substrates, the slides were kept in a solution of Fab′ fragments for 2 h, followed by 18 h in a BSA solution and 2 h in a hIgG solution. Substrates were gathered from each coating step, rinsed with high-purity water and air-dried. The slides were kept dry at room temperature until the imaging was performed.

Nanoscope II and III (Digital Instruments, Santa Barbara, CA) atomic force microscopes in contact and tapping mode, respectively, were used for imaging the sample surfaces in ambient air. An A-scanner (1×1 μm^2 scan range) with standard Nanoprobe silicon nitride cantilevers supplied by the manufacturer (force constant of $k=0.06$ Nm^{-1}) was used for contact mode imaging. A J-scanner (150×150 μm^2 scan range) with silicon cantilevers (TESP) supplied by the manufacturer (Nanoprobes) was used for tapping mode imaging. The free amplitude of the cantilever (off contact) was chosen to be 30 nm. Some test measurements were also performed using a free amplitude of 100 nm, but no pronounced differences in image contrast were observed. The engage procedure causes a shift in the resonance frequency of the cantilever. This was taken into account and the new resonance frequency for the tip in contact was determined and used as the operating frequency. Light

to moderate tapping, with a damping ratio (contact amplitude/free amplitude) of about 0.6–0.9 was used for imaging, the main criterium being not to modify the sample surface.

2.5. The quartz crystal microbalance

The change in frequency due to the attachment of proteins to the lipid layer was measured with a 10 MHz QCM as previously described [10]. The mass of the proteins was estimated according to Sauerbrey's equation, where the observed decrease in resonant frequency, f_0, is proportional to the change in mass, δ_m, of the quartz resonator, i.e.

$$\delta f = \frac{-2f_0^2\delta_m}{A\sqrt{\rho_q\mu_q}} \quad (1)$$

A denotes the electrode area, ρ_q the density of quartz and μ_q the shear modulus of quartz. The resonators were purchased from Universal Sensors (Louisiana, USA). The edges of the resonators were covered with a ring of silicone rubber (Dow Corning), which prevented corrosion of the wires and degradation of the electrical contacts when submerged in solution. A Hewlett–Packard 4195A spectrum/network analyser connected to a computer was used as earlier described [8,33]. The gold electrode was cleaned with chromosulphuric acid, rinsed with water and air-dried before the measurements. The same crystal was used repeatedly. The QCM was horizontally lowered to make contact with the lipid monolayer (Fig. 1a). Buffer solution was pumped through the measuring cell placed below the QCM with a flow rate of 1 ml/min for about 3 min. The pump was stopped and when a stable baseline was reached protein solution was added into the cell. All experiments were performed at a temperature of 21°C.

2.6. Surface plasmon resonance

The SPR configuration used in this study has been described by Sadowski et al. (Fig. 1b) [35]. Linearly *p*-polarised light of a wavelength of 632.8 nm from a He–Ne laser is directed through a prism onto a slide coated with a thin gold film positioned according to the Kretschmann configuration [36]. The intensity of the light is measured as a function of time at the particular angle where light is partly in resonance. Very small changes in light levels can be measured by using two lock-in amplifiers at two different chopping frequencies to monitor light from the prism (sample beam) and from the laser (reference beam). Although in this case the dynamic range of SPR detection is limited, the method is particularly suited for measurements in liquid, where the resonance peak is rather broad. The Au/ODM-substrates with the deposited monolayer matrix were attached to the prism via an index matching oil. A flow cell was placed over the measurement area of the film and was filled with buffer. Protein solutions were pumped into the cell and changes in the intensity of the light were detected for about 10–15 min at a suitable angle of incidence. The surface was rinsed with buffer between every injection of protein in order to determine the amount of bound protein. The intensity was allowed to stabilise and the difference between the levels was recorded.

2.7. Radioimmunoassay

The linker lipid embedded in a host monolayer matrix of DPPC (or DPPC/CHOL) was deposited on Si/ODTCS substrates. Anti-human Fab′ (50 μg/ml in HEPES buffer, pH 6.8) was subsequently bound to the layers in 2 h at room temperature using a thin film reaction chamber with a volume of 30 μl. The slides were hereafter transferred to a PBS buffer (0.15 M NaCl, 10 mM KH_2PO_4, pH 7.5) containing 0.5 g/l BSA (bovine serum albumin, Sigma RIA grade) and left in this solution at 4°C for 18 h. Series of silicon slides were then incubated with increasing standardised amounts of hIgG in the presence of a constant amount of ^{125}I-labelled hIgG and BSA (3.3–5.0 g/l). The amount of Fab′ immobilised was assessed also by a standardised radiotracer method, using ^{125}I-labelled Fab′.

3. Results and discussion

3.1. Lipid monolayer formation

The extrapolated mean molecular area (Mma) for the compressed monolayers of CHOL, DPPC and DPPE-EMC was determined from surface pressure–

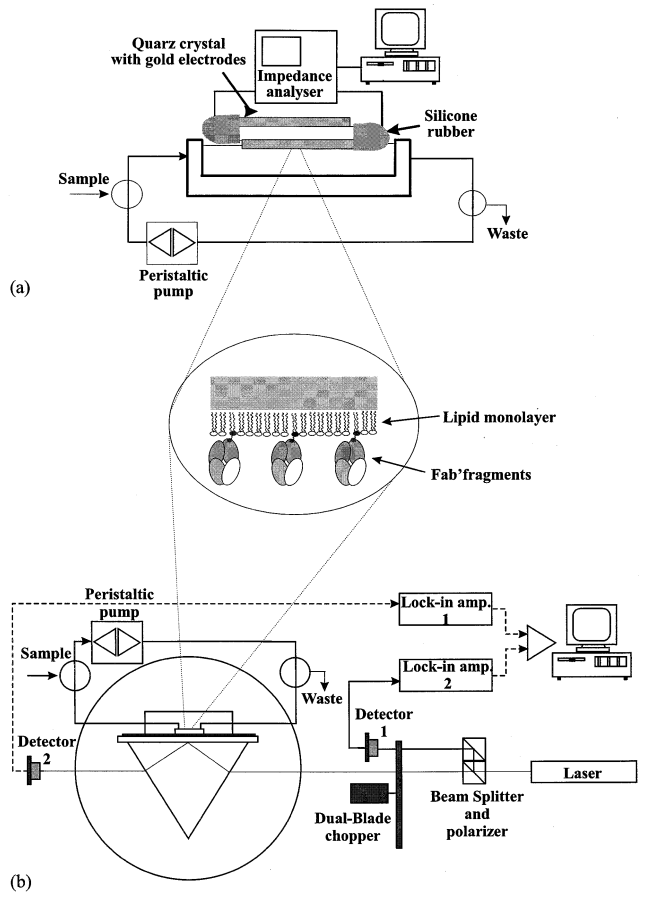

Fig. 1. Schematic view of the QCM (a) and SPR (b) measuring set-up. The QCM was lowered to make contact with the Langmuir layer and protein solution was pumped into a flow cell placed below the crystal. In the SPR measurements, the monolayer was transferred onto an Au/ODM slide which was subsequently attached to a glass prism.

area isotherms as 37 ± 2, 50 ± 3 and 112 ± 5 Å^2/molecule, respectively (data not shown). The Mma of CHOL and DPPC were in good agreement with the values reported in the literature. The Mma for the DPPE-EMC is larger than that of the DPPC monolayer. This is likely due to an increase in size of the molecule and an increase in electrostatic repulsion [37,38]. DPPE-EMC is negatively charged, while DPPC has a zwitterionic head group. The Mma of the matrices used in this study (DPPC/DPPE-EMC and DPPC/DPPE-EMC/CHOL) was 54 ± 3 and 43 ± 2 Å^2/molecule, respectively. This clearly shows the condensing effect of CHOL. The hydrophobic steroid ring of cholesterol has been proposed to be oriented parallel to the alkyl chains of the phospholipids, with the hydroxyl group in the close vicinity of the phospholipid ester carbonyl group and the isooctyl side chain deeply buried in the acyl chain domain [39]. When ideal mixing of DPPC and DPPE-EMC is assumed the total area per linker lipid can be estimated to be 102.5 Å^2 at a surface pressure of 40 mN/m [10].

3.2. Binding of Fab′ to the lipid monolayers

With SPR, a fast interaction of the Fab′ with the DPPC/DPPE-EMC monolayer could be observed, when Fab′ fragments were pumped into the flow cell. Saturation was reached within 10 min (Fig. 2). A slight decrease in the intensity was observed when buffer was injected after the Fab′ fragments. This indicates that some of the Fab′ fragments were non-specifically bound and were washed away during the buffer rinsing or there might be a small change in the bulk refractive index. When BSA was added, an increase in intensity was again observed, after rinsing with buffer the signal again decreased. The BSA adsorption was much higher for the layer with CHOL. If the DPPC/DPPE-EMC layer was allowed to interact with goat anti-human $F(ab')_2$ there was no shift in the light intensity of the SPR or change in resonant frequency of the QCM (data not shown). This confirms that the binding of Fab′ to the linker was achieved via the free thiol groups to the maleimide.

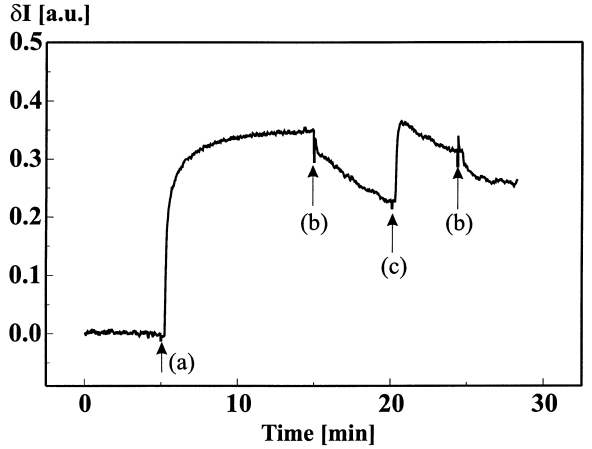

Fig. 2. Shift in SPR intensity on interaction of 56 μl/mg Fab′ fragments with DPPC/DPPE-EMC. The consecutive steps can be distinguished: linking of the antibody (a), rinsing with buffer (b) and non-specific adsorption of BSA (c).

The SPR intensity response was dependent on the Fab′ fragment concentration (Fig. 3a). The change of reflection intensity was directly proportional to the surface coverage and when a homogeneous distribution of Fab′ fragments was assumed, fitting to a Langmuir adsorption isotherm could be used to calculate the apparent association constant, K_a, for the binding of Fab′ fragments to the monolayer. The inset in Fig. 3a gives a binding constant of 1.6 (± 0.5)$\times 10^5$ M^{-1} ($R = 0.955$) for the DPPC/DPPE-EMC monolayer. A much higher binding constant was found for the matrix containing cholesterol, reaching a value of 1.0 (± 0.8)$\times 10^7$ M^{-1} ($R = 0.991$).

Measurements with the QCM at the air–water interface gave a decrease in the resonant frequency upon binding of Fab′ fragments to the lipid layer [10,33]. The binding constant of 1.2 (± 0.5)$\times 10^7$ M^{-1} ($R = 0.965$) for the DPPC/DPPE-EMC monolayer was much higher than that measured with SPR. The large difference is at the moment not clear, but may be a consequence of the fact that the SPR measurements were performed on a layer that had been transferred onto the hydrophobic Au/ODM slides and stored dry, whereas the QCM measurements were performed in situ at the air–water interface. The transfer of the layer might change the orientation of the linker groups and, moreover, the lipid film most probably reoriented when it was stored in air.

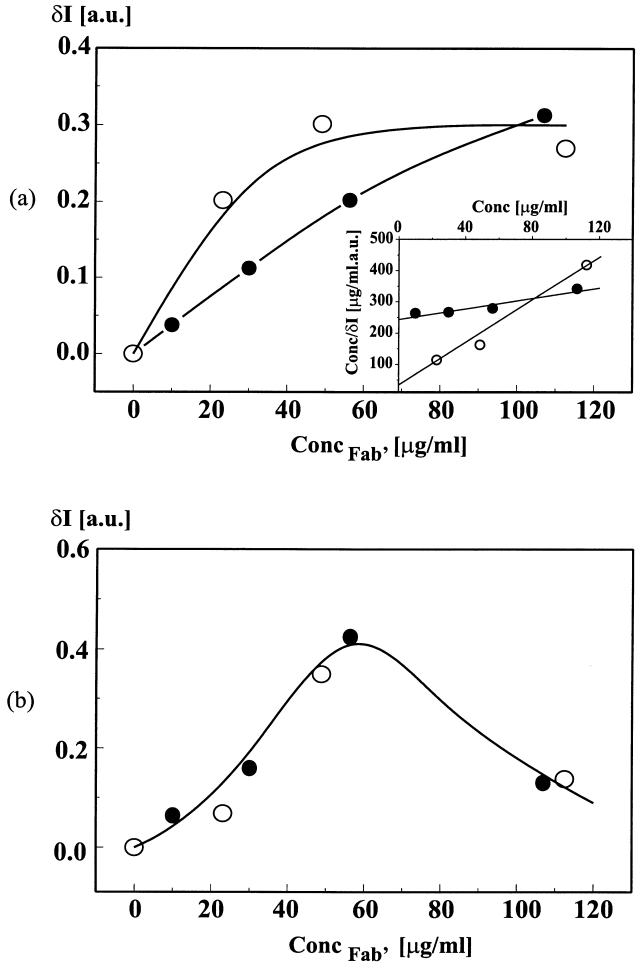

Fig. 3. The total change in the reflected SPR light intensity upon binding of (a) Fab′ fragments and (b) the subsequent binding of hIgG to a monolayer of DPPC/DPPE-EMC (●) and DPPC/DPPE-EMC/CHOL (○) as a function of Fab′ fragment concentration. The reproducibility of the measurements range within 5 and 10% for the DPPC/DPPE-EMC and DPPC/DPPE-EMC/CHOL matrix, respectively.

3.3. Binding efficiency of immobilised Fab′ fragments

The binding of the antigen hIgG to the immobilised Fab′ as studied with QCM and SPR was of Langmuir type. A binding constant of 2×10^7 M^{-1} was determined for the DPPC/DPPE-EMC layer (Table 1). A 10-fold higher binding constant was obtained with SPR for the CHOL matrix. This might be due to the higher amount of non-specific binding to this matrix as discussed later. The total amount of human IgG bound was dependent on the amount of Fab′ bound to the layer (Fig. 3b). The amount of hIgG bound increased with Fab′ concentration and reached a maximum at about 60 μg/ml for both matrices. The density of Fab′ on the matrix containing CHOL was higher than on the DPPC/DPPE-EMC matrix, but the binding capacity for hIgG was about the same, yielding a lower binding efficiency of the CHOL matrix (Table 2). This is in agreement with

Table 1
Apparent binding constants, at a Fab′ fragment concentration of 50 μg/ml, for the binding of hIgG to Fab′ in various monolayer matrices measured with SPR and QCM

Monolayer matrix	K_a (M^{-1})	
	SPR	QCM
DPPC/DPPE-EMC	1.8×10^7	2.0×10^7
DPPC/DPPE-EMC/CHOL	1.2×10^8	2.6×10^7

S.D. = 0.5×10^7 M^{-1}.

our earlier RIA measurements which have shown that higher amounts of Fab′ can be attached to a matrix containing CHOL, but that the increase in binding capacity is very small [10]. SPR measurements also correlated with the QCM results, which showed that the binding of BSA was higher when CHOL was included in the matrix. The reduction in hIgG binding efficiency of the CHOL matrix is thus caused by an unfavourable orientation of Fab′. This conclusion is further supported by the fact that QCM, SPR, and RIA measurements gave very similar binding efficiencies for the DPPC/DPPE-EMC monolayer (Table 2), while a large divergence was seen for the binding efficiencies of the DPPC/CHOL/DPPE-EMC monolayer. This was also the case for the binding constant (Table 1).

Crystallographic dimensions of about $7\times5\times4$ nm^3 have been reported for the Fab′ fragment [40]. The height of a Fab′-monolayer can thus vary between 4 and 7 nm depending on whether the fragment is bound in a side-on (4 nm), edge-on (5 nm) or end-on (7 nm) orientation. A closely packed layer would have a surface mass density varying between 220 and 440 ng/cm^2 (220 ng/cm^2 for side-on, 355 ng/cm^2 for edge-on and 390–440 ng/cm^2 for end-on orientation) [41]. We found that at an optimal concentration of Fab′ the QCM showed a resonant frequency of change of 70 Hz on attachment of antibody fragments to the DPPC/DPPE-EMC monolayer (data not shown). Proteins possess a considerable amount of water and this will contribute to the frequency response [8,10]. When 30% of the frequency shift is assumed to be due to hydration water [42], the 70 Hz frequency-change would correspond to a surface mass density of about 200 ng/cm^2. The high binding efficiency of 62.5% (Table 2), indicates that most of the Fab′ fragments are standing end-on and take up about half of a tightly packed monolayer. Fab′ fragments with a surface density of 6.3×10^{11} molecules/cm^2 have been immobilised onto plasma-polymerised layers via maleimide [30]. This would correspond to about 50 ng/cm^2, which is only 13% of that of a tightly packed Fab′-layer with molecules standing end-on. Shriver-Lake et al. reported surface densities and immobilisation efficiencies for whole antibody molecules immobilised by various heterobifunctional crosslinkers onto glass [26]. For succinimide coupling optimal densities between 100 and 220 ng/cm^2 were found with binding efficiencies between 8 and 18.5%. The site-directed, more oriented hydrazide coupling gave an antibody density of 160 ng/cm^2 and a binding efficiency of up to 18.5%[2].

Table 2
Binding efficiency, η_a of Fab′ fragments, attached to linker lipids at a concentration of 50 μg/ml, for hIgG as measured with QCM, SPR, RIA and AFM

Monolayer matrix	η_a (%)				
	QCM	SPR	RIA	AFM[a]	
				Contact	Tapping
DPPC/DPPE-EMC	62.5	65.9	60	48	58
DPPC/DPPE-EMC/CHOL	58.6	36.4	24	–	55

[a]The binding efficiency was estimated from the total surface coverage of the globular objects observed on the Fab′ fragment and hIgG-coated samples.

3.4. Morphology of the deposited films

In order to obtain more detailed information on the orientation of the Fab′ fragments and the antigen hIgG, the plain monolayers and those being exposed to Fab′ fragments and consequently to BSA and hIgG were imaged with AFM (Table 3). Both contact and tapping mode imaging were used. The clear advantage of tapping mode is that the tip-sample lateral forces present in contact mode imaging are to a large extent eliminated and thus the risk of destruction of the soft organic film or reorientation of the biomolecules by the tip can be minimised. The comparative measurements of tapping mode vs. contact mode were, therefore, expected to give extra information about the mechanical properties and stability of the monolayer structures.

The DPPC/DPPE-EMC monolayer imaged in contact mode was relatively smooth with a few holes of bilayer thickness (Fig. 4a, left). Tapping mode imaging of the same monolayer revealed not only the

[2] The reported values of Shiver-Lake et al. [26] for the antigen/antibody ratio were here divided by two since one IgG antibody can bind two antigens.

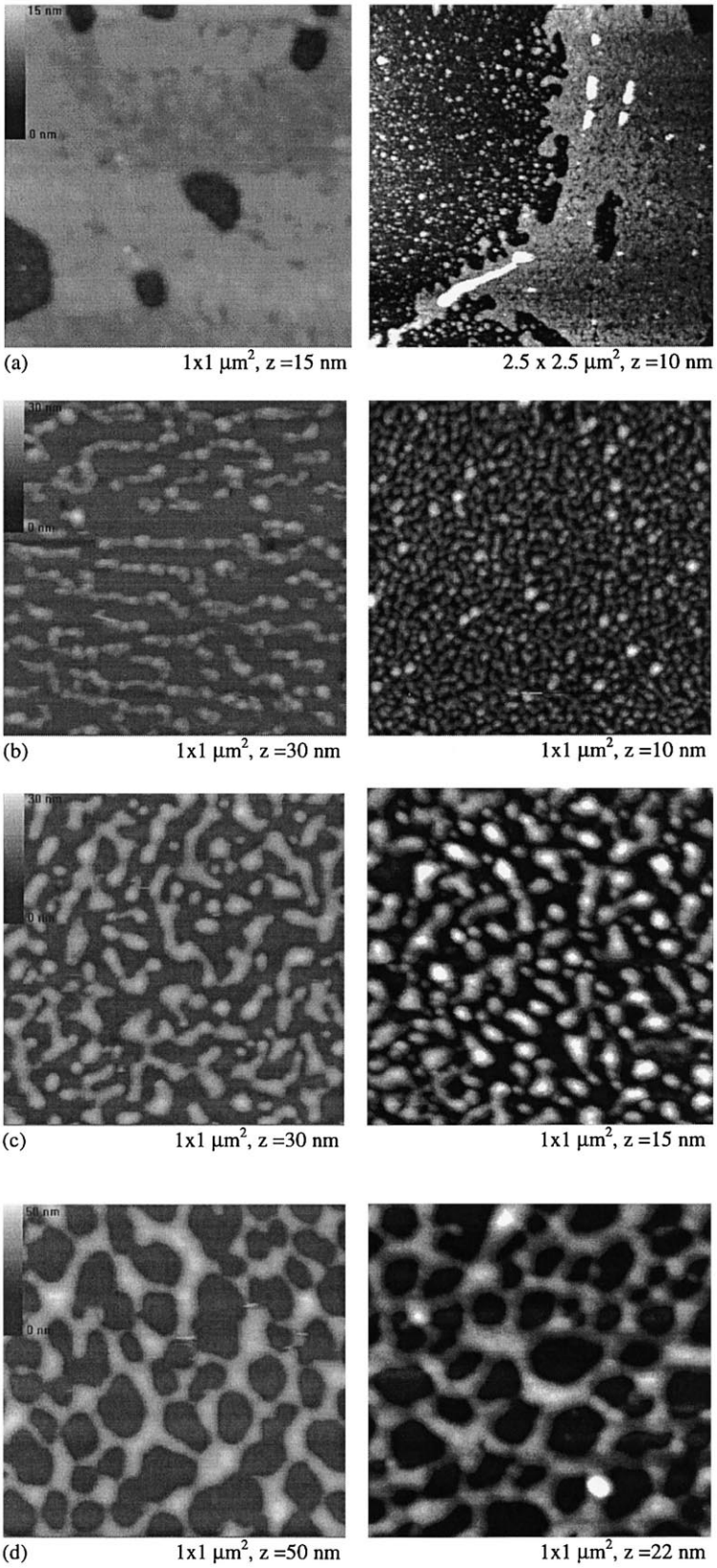

(a) 1x1 μm², z =15 nm

2.5 x 2.5 μm², z =10 nm

(b) 1x1 μm², z =30 nm

1x1 μm², z =10 nm

(c) 1x1 μm², z =30 nm

1x1 μm², z =15 nm

(d) 1x1 μm², z =50 nm

1x1 μm², z =22 nm

Table 3
Characteristics of Fab′ fragments, BSA and hIgG obtained from AFM

Monolayer matrix	Monolayer		Fab′ fragments	
	Height (nm)	Coverage (%)	Height (nm)	Coverage[a] (%)
DPPC/DPPE-EMC	6 ± 0.5 7.7 ± 0.8	–	4.2 ± 0.7 7.5 ± 0.5	51 ± 1 (34 ± 2)
DPPC/DPPE-EMC/CHOL	3–7	–	5.7 ± 0.6 8.5 ± 1.2	42 ± 2
	BSA		Human IgG	
	Height (nm)	Coverage[a] %	Height (nm)	Coverage[a] %
DPPC/DPPE-EMC	5.2 ± 0.8 9 ± 1	51 ± 2 (43 ± 1)	8.4 ± 0.8 13 ± 2	50 ± 1 (41 ± 1)
DPPC/DPPE-EMC/CHOL	3–5	∼100	8.4 ± 0.9 12.2 ± 0.9	53 ± 1

[a]The values in parentheses are obtained from contact mode images.

bilayer region with holes with a depth of 6.2 ± 0.4 nm, but also another characteristic region consisting of globular objects with a height of 6 ± 0.5 and 7.7 ± 0.8 nm (Fig. 4a, right and Table 3). These objects were likely quite loosely bound to the substrate. This occasionally made the measurement unstable, i.e. it was quite difficult to optimise the measurement conditions and avoid drift and noise. In contact mode this problem did not appear, most probably because the tip displaced the globular objects during scanning. The almost equal dimensions of the globular objects and the holes of the bilayer structures indicate that the spheres are micelles formed as a result of a film-to-particle reorganisation. Budded vesicles have been observed on phosphatidylcholine bilayers, whereas layers containing cholesterol have shown to be stable [43]. Those layers were, however, stored in an aqueous environment, whereas these layers were stored dried in air. The stability of the monolayer is determined by the balance of strength of repulsive forces within the monolayer and between the lipid monolayer and the alkylsilane layer. The kinetics of reorganisation of the monolayers in Fig. 4a was not studied in more detail here, but the reorganisation of the monolayer took most probably place immediately after the samples were removed from the subphase after deposition. No bilayer structures or globular objects could be found on the Si/ODTCS substrates used as a solid support for the lipid matrices. On the contrary, these substrates looked very smooth with a characteristic roughness of ca. 0.46 ± 0.03 nm (see for comparison Fig. 7a).

Stripes of globular features were observed in contact mode for the DPPC/DPPE-EMC monolayer that was allowed to interact with Fab′ fragments (DPPC/DPPE-EMC/ Fab′, Fig. 4b, left). The stripes were oriented parallel to the quick scanning direction and were likely effected by the AFM tip. However, the topography of the sample did not change after the surface was scanned repeatedly up and down. This indicates that if non-specifically bound Fab′ fragments were present on the surface, they were swept away by the tip, while other globular objects remained on their position, and were assigned to be covalently bound Fab′ fragments. In tapping mode, small globular objects with lateral dimensions of 20–80 nm and height of 4.2 ± 0.7 and 7.5 ± 0.5 nm were observed (Fig. 4b, right and Table 3). The height of these objects was almost the same as for those observed for the plain monolayer (Table 3), but the amount of the objects had increased significantly to cover almost the whole surface. It is possible that

←
Fig. 4. AFM images of Si/ODTCS slides coated with a monolayer of (a) DPPC/DPPE-EMC, (b) after interaction with Fab′ fragments at a concentration of 50 μg/ml, (c) 0.1 mg/ml BSA and (d) 0.1 mg/ml human IgG. The AFM images on the left are measured in contact mode and the ones on the right in tapping mode.

some of the smaller objects were aggregated lipids, but the majority of the objects is believed to be Fab′ fragments attached on the surface in a slightly slanted or right-up position and being partly aggregated. This conclusion has been drawn on the basis of the size of a Fab′ ($7\times5\times4$ nm^3) [40] and that the tip-sample convolution and distortion of the molecules under the scanning tip usually tends to exaggerate the size of the imaged objects [44]. The much higher surface coverage of the globular objects observed when using tapping mode probably originates from the minimal lateral force that was not high enough to displace the non-covalently bound Fab′ fragments and/or aggregates/flattened micelles from the monolayer.

Addition of BSA (DPPC/DPPE-EMC/Fab′/BSA) made the stripes observed in the contact mode image slightly larger and the linearity parallel to the quick scan axis had disappeared (Fig. 4c, left). Exactly the same features were observed with tapping mode imaging (Fig. 4c, right). The size of the objects increased from 20–80 nm for the surface coated by the antibody to 35–400 nm after the BSA adsorption and the height increased from 4.2 ± 0.7 and 7.5 ± 0.5 nm to 5.2 ± 0.8 and 9 ± 1 nm (Table 3). The deep areas refer to the lipid monolayer surface free of any protein. The increase of this deep regime refers to the desorption of non-specifically bound Fab′ fragments being only partly replaced by BSA. This phenomenon was also occasionally observed in SPR measurements (data not shown). The increase of the object size indicates that the BSA molecules end up in a slightly slanted orientation in the vicinity of the Fab′ fragments, but not on top of the Fab′ fragments due to only small changes in the height differences. The conclusions are based on the fact that BSA has an ellipsoidal structure with dimensions of $11.6\times2.7\times2.7$ nm^3 [45]. Furthermore, the efficiency of the Fab′ fragments to bind hIgG remained high.

Human IgG formed a network with a height variance of 8.4 ± 0.8 and 13 ± 2 nm on the DPPC/DPPE-EMC/ Fab′/BSA matrix (Fig. 4d and Table 3). The network structure was independent of the imaging mode and was highest in the crossings. These dimensions correspond to the hIgG standing end-on with the arms bound to another antigen at the crossings. This picture is also supported by the fact that the average height does not exceed 14 nm, which is the maximum height for an IgG molecule [42]. The network structure formed by hIgG correlates quite well with the surface structure after BSA adsorption although the area covered by the hIgG network is slightly lower than that left free after BSA immobilisation. Despite this the Fab′ fragments have obviously retained a high binding efficiency, especially if one compares the contact mode and tapping mode images of the Si/ODTCS/lipid monolayer substrates being exposed to Fab′, BSA and hIgG solutions.

The hIgG binding efficiency of the Fab′ fragments was estimated to be about 50 and 60% determined from the tapping mode and contact mode images, respectively. Tapping mode images generally showed a higher surface coverage of proteins than the contact mode images because the tapping mode images include a larger amount of non-specifically bound proteins for the reason discussed earlier. These values correspond well to the values observed with SPR, QCM and RIA (Table 2). The surface coverage of the proteins was roughly estimated from a mean area per protein. An area of about 31 and 64 nm^2 was obtained for one Fab′ fragment (dimensions, $7\times5\times4$ nm^3) [40] and one IgG (dimensions, $14\times8.5\times4$ nm^3) [42], respectively. This determination of the IgG binding efficiency via AFM is rather simplified but gave reasonable values.

Globular objects, but no holes of bilayer thickness were observed in the tapping mode images of the DPPC/CHOL/DPPE-EMC monolayer matrix deposited on a Si/ODTCS substrate (Fig. 5a). The height of the spherical objects varied between 3 and 7 nm, thus referring to either micellar or hemimicellar structures. One explanation for these objects could be that the DPPC and DPPE-EMC molecules were squeezed out from the monolayer because of the very stiff nature of cholesterol. Globular objects with different morphology were observed as a result of Fab′ fragment immobilisation (Fig. 5b). The size of the objects was almost the same as in the case of the DPPC/DPPE-EMC matrix. Addition of BSA made the DPPC/CHOL/DPPE-EMC/Fab′ surface very smooth (Fig. 5c). Some holes with a depth of 1.5–5 nm are occasionally present in the layer. The larger globular objects had a height of 5–8 nm and the small crowned objects that dominated the image had a height of 1.5–4 nm. After interaction with hIgG large globular objects with heights of 8.4 ± 0.9

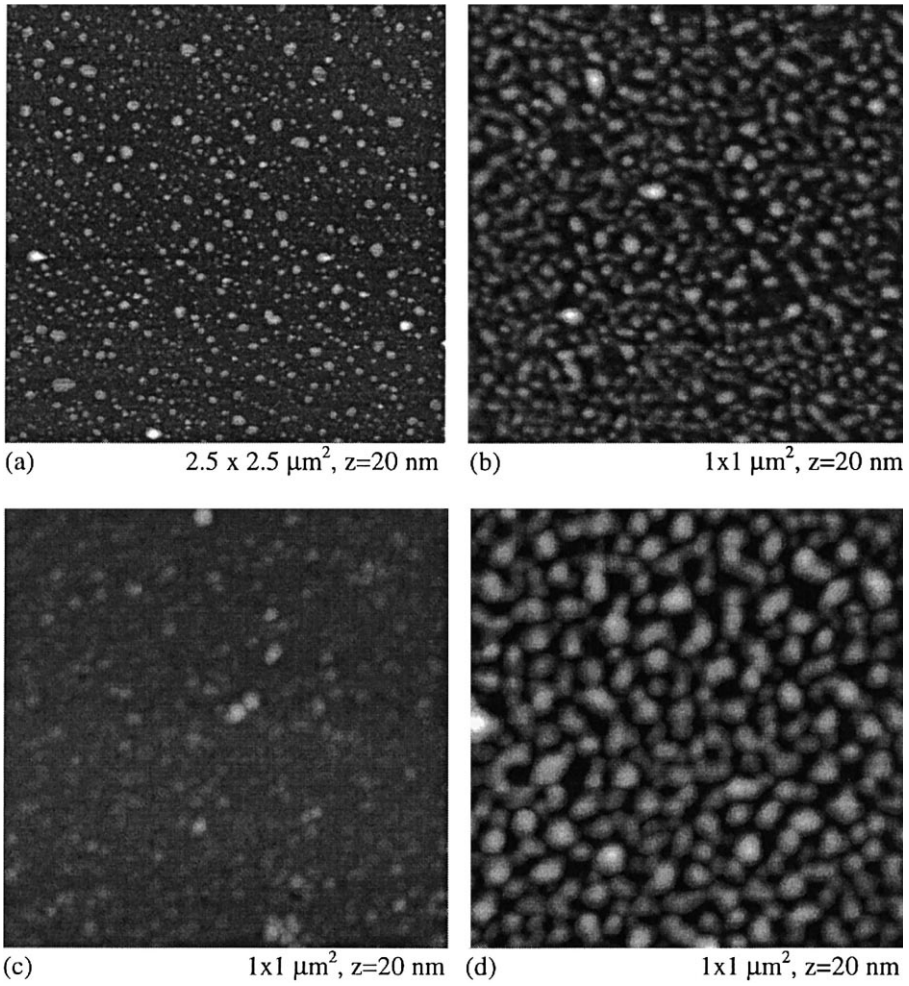

Fig. 5. Tapping mode AFM images of Si/ODTCS slides coated with a monolayer of (a) DPPC/DPPE-EMC/CHOL, (b) after interaction with Fab′ fragments at a concentration of 50 μg/ml, (c) 0.1 mg/ml BSA and (d) 0.1 mg/ml human IgG.

and 12.2 ± 0.9 nm were visible. The heights correspond to hIgG in a slightly tilted or upright position, respectively. However, no network structure was formed. The network formation might be a result of the higher fluidity of the DPPC/DPPE-EMC matrix. The hIgG binding efficiency of Fab′ as determined from the surface coverage was about 55%, which is much larger than the value obtained by SPR, QCM and RIA. This indicates that non-specific binding of proteins to the DPPC/CHOL/DPPE-EMC matrix is higher than to the DPPC/DPPE-EMC matrix. This was also seen from the QCM and SPR measurements where more BSA was adsorbed to the DPPC/CHOL/DPPE-EMC/Fab′ layer than to the DPPC/DPPE-EMC/Fab′ layer. The reason for this probably lies in the charge of DPPC, which is more shielded by bulky groups in the polar head group than the charge in the polar region of CHOL. The electrostatic interaction between BSA and the lipid matrix containing CHOL would then be stronger than between BSA and the lipid matrix without CHOL, leading to higher non-specific adsorption of BSA to the former one. We have also noticed that the non-specific adsorption of BSA has been higher to lipid matrices with phosphoethanolamines than to matrices containing phosphatidylcholine, which further supports the above conclusion.

The contact mode measurements performed for the samples prepared on the DPPC/CHOL/DPPE-EMC matrix were difficult to carry out (no images shown). The tip modified the surface even after several scans, which was not the case with the DPPC/

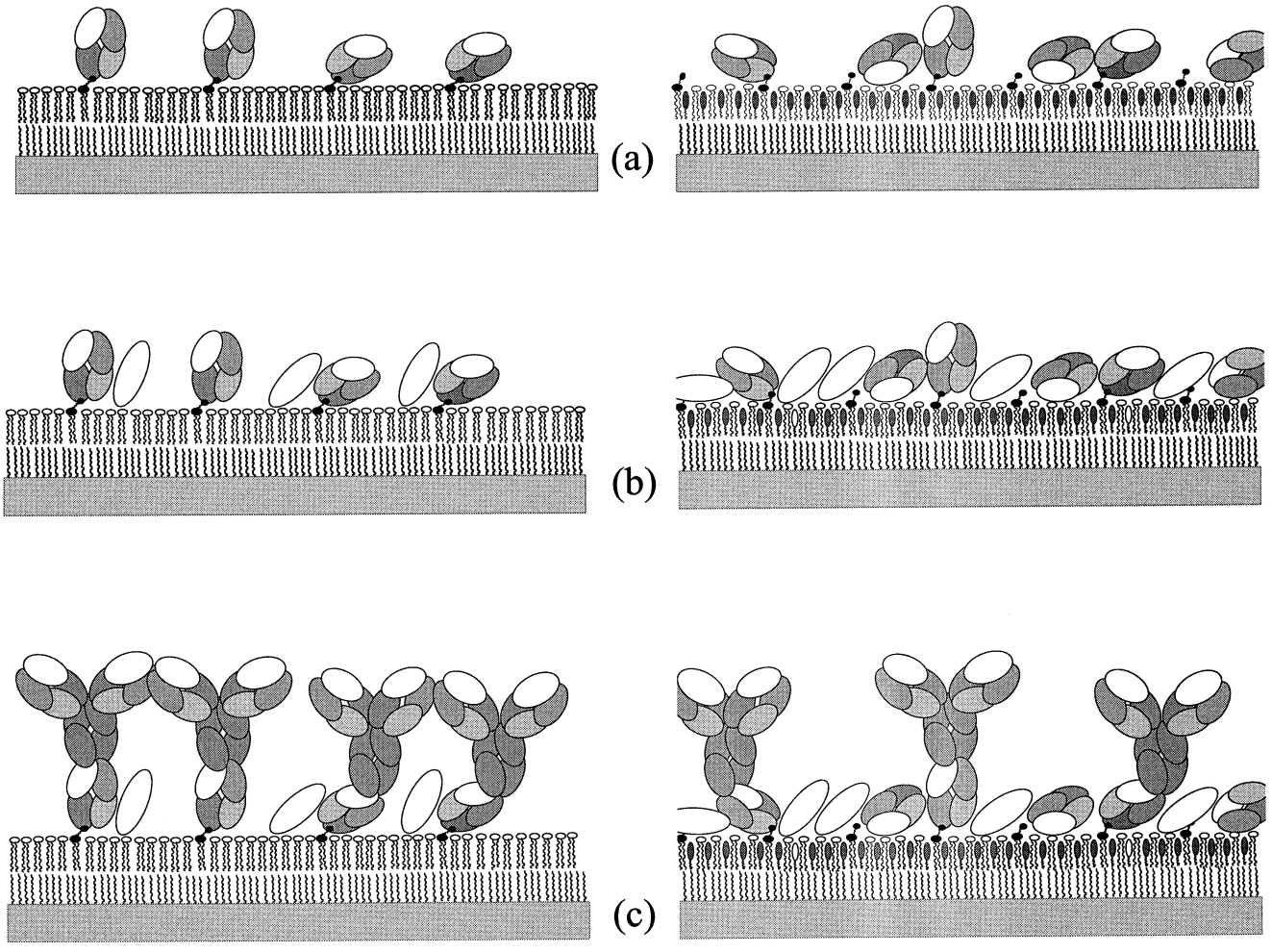

Fig. 6. A simplified schematic view of the immobilisation procedure. (a) Attachment of Fab′ fragments to the linker lipids in the matrix monolayer. (b) Non-specific binding of BSA. (c) Binding of human IgG. The monolayer with cholesterol (DPPC/CHOL/DPPE-EMC to the right) showed a higher binding for Fab′ and non-specific binding for BSA compared to the layer without cholesterol (DPPC/DPPE-EMC matrix to the left). The binding capacity of the Fab′ fragments for hIgG was, however, about the same for both layers, indicating a lower binding efficiency for the DPPC/CHOL/DPPE-EMC layer.

DPPE-EMC matrix. The binding efficiency for this matrix could therefore not be estimated from the contact mode images. This also supports our conclusion that the proteins are much more readily adsorbed non-specifically to the DPPC/CHOL/DPPE-EMC matrix than to the DPPC/DPPE-EMC matrix. A simplified schematic representation of the suggested immobilisation of the Fab′ fragments, BSA and human IgG onto the studied films is illustrated in Fig. 6.

A large amount of Fab′ fragments were attached to the Si/ODTCS/lipid monolayer surface, even after the substrates had been dried and stored in air. This indicates that some dissolution of the upper layer of the formed bilayer or re-attachment of the monolayer on the solid substrate took place when the air dried substrates were submerged in the Fab′ fragment solution. This conclusion is supported by the following facts: (1) the bilayer structures observed for the deposited films were not observed after interaction with Fab′ fragments; (2) occasionally, large round areas where the proteins had aggregated into a thread-like network structure were observed (Fig. 7b). These aggregated structures resemble the struc-

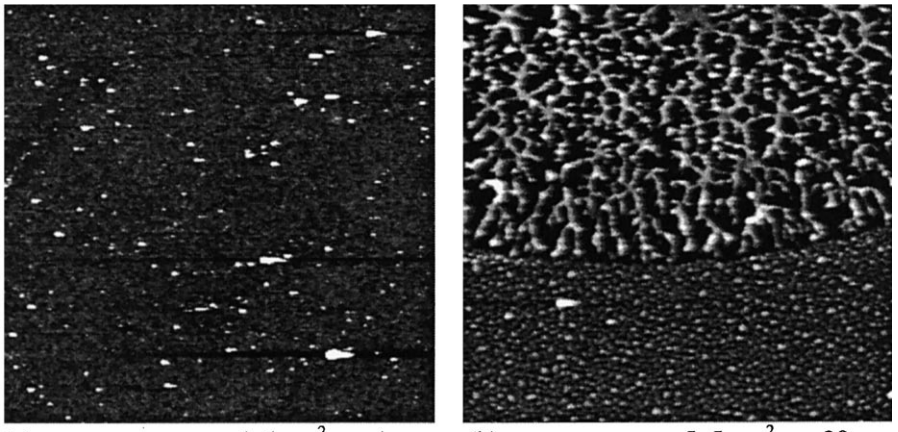

Fig. 7. Tapping mode AFM images of (a) a pure Si/ODTCS surface and (b) a DPPC/DPPE-EMC monolayer after incubation in Fab′ fragment, BSA and IgG solutions showing the occasionally found thread-like structure.

tures seen by Wälivaara et al. [46] for non-specifically bound IgG to a methylated Si surface; and (3) both the QCM and SPR measurements showed low non-specific binding of $F(ab')_2$ and a high specific binding of Fab′ fragments, even though the QCM measures protein attachment in situ on a floating monolayer while SPR is used for the analysis of solid supported monolayers at the solid/liquid interface.

4. Conclusions

In the design of immunosensors strict control over the immobilisation conditions and the possibility to control the surface properties is very important. The covalent coupling of antibodies to a linker lipid in monolayer matrices produced by the Langmuir–Blodgett film technique have successfully been demonstrated. The surface density and orientation of the fragments were largely dependent on the lipid matrix composition. The activity of the immobilised antibodies could be investigated with many different techniques, both microscopic and macroscopic. QCM detection, radioassay methods, SPR and AFM form a very good set of characterisation methods for a more intricate study of structure and function of biomolecular films, as demonstrated here for the model system hIgG. It appears that interfacial aspects, when well-controlled, can be used in a positive way for optimisation of orientation and functionality of antibodies, in terms of capacity and affinity constants. Additional advantages were obtained by comparing the results of measurements made in situ (QCM) with those of transferred films (radioimmunoassay and SPR) and by comparing AFM results obtained via contact mode and tapping mode.

The deposition of the monolayers in conjunction with the dry storage lowered the reactivity of the linker lipid to the antibody fragments. Despite this, the antigen binding efficiency of the antibodies determined by all the used techniques was very similar for the DPPC/DPPE-EMC lipid matrix while in the case of the DPPC/CHOL/DPPE-EMC lipid matrix the efficiency varied depending on the used measuring technique. This may also be caused by the higher degree of non-specific binding of the monolayers with cholesterol and differences in fluidity of the layers. The Fab′, BSA and hIgG layers were identified by performing a height analysis of the sample surface after the immobilisation procedures. The non-specific protein adsorption to the lipid layers was also revealed by comparative measurements made in contact and tapping modes.

As the transfer process, rinsing and drying of the deposited monolayers affected the properties and reactivity of the linker lipids, we are presently imaging the in situ binding of Fab′ fragments of monoclonal antibodies to the deposited lipid matrices in a buffer solution. Preliminary binding studies of monoclonal Fab′s to the DPPC/DPPE-EMC monolayer have been encouraging.

Acknowledgements

This work was financed by the Technology Development Centre of Finland, the Academy of Finland and the Technical Research Centre of Finland.

References

[1] S. Löfås, M. Malmqvist, I. Rönnberg, M. Stenberg, B. Liedberg, I. Lundström, Sens. Act. B 5 (1991) 79–84.
[2] J.E. Roederer, G.J. Bastiaans, Anal. Chem. 55 (1983) 2333–2336.
[3] J. Harteveld, M. Nieuwenhuizen, E. Wils, Biosens. Bioelectron. 12 (1997) 661–667.
[4] A. Perrin, V. Lanet, A. Theretz, Langmuir 13 (1997) 2557–2563.
[5] M. Liley, J. Bouvier, H. Vogel, J. Colloid Interface Sci. 194 (1997) 53–58.
[6] Th. Wink, S.J. van Zuilen, A. Bult, W.P. van Bennekom, Anal. Chem. 70 (1998) 827–832.
[7] G. Sauerbrey, Z. Phys. 155 (1959) 206–213.
[8] J. Rickert, A. Brecht, W. Göpel, Anal. Chem. 69 (1997) 1441–1448.
[9] H. Välimäki, J. Lekkala, H. Helle, Sens. Act. A 60 (1997) 80–85.
[10] I. Vikholm, W.M. Albers, Langmuir 14 (1998) 3865–3872.
[11] D.E. Nivens, J.Q. Chambers, T.R. Anderson, D. White, Anal Chem. 65 (1993) 65–69.
[12] B. Rothenhausler, C. Duschl, W. Knoll, Thin Solid Films 159 (1988) 323–330.
[13] S. Terrettaz, T. Stora, C. Duschl, H. Vogel, Langmuir 9 (1993) 1361–1369.
[14] L. Häussling, H. Ringsdorf, F. Schmidt, W. Knoll, Langmuir 7 (1991) 1837–1840.
[15] B. Lu, M.R. Smyth, R. ÓKennedy, Analyst 121 (1996) 29R–32R.
[16] B. Attili, A. Suleiman, Microchem. J. 54 (1996) 174–179.
[17] F. Caruso, E. Rodda, D.N. Furlong, J. Colloid Interf. Sci. 178 (1996) 104–115.
[18] W.L. Hoffman, D.J. ÓShannessy, J. Immunol. Methods 11 (1988) 113–120.
[19] J. Lekkala, J. Sadowski, in: Chemical Sensor Technology, Vol. 5, Aizawa, 1994, pp. 199–213.
[20] B. Fischer, S.P. Heyn, M. Egger, H.E. Gaub, Langmuir 9 (1993) 136–140.
[21] M. Schönhoff, M. Lösche, M. Meyer, C. Wilhelm, Progr. Colloid Polym. Sci. 89 (1992) 243–248.
[22] U.J. Krull, R.S. Brown, E.T. Vandenberg, W.M. Heckl, J. Electr. Microsc. Techn. 18 (1991) 212–222.
[23] S.P. Heyn, M. Egger, H.E. Gaub, J. Phys. Chem. 94 (1990) 5073–5078.
[24] I. Vikholm, E. Györvary, J. Peltonen, Langmuir 12 (1996) 3276–3281.
[25] H. Morgan, D.M. Taylor, Biosens. Bioelectron. 7 (1992) 405–410.
[26] L.C. Shriver-Lake, B. Donner, R. Edelstein, K. Breslin, S.K. Bhatia, F.S. Ligler, Biosens. Bioelectron. 12 (1997) 1101–1106.
[27] D.M. Disley, D.C. Cullen, H.-X. You, C.R. Lowe, Biosens. Bioelectron. 13 (1998) 1213–1225.
[28] A. Ahluwalia, M. Carra, D. De Rossi, C. Ristori, P. Tundo, A. Bomben, Thin Solid Films 247 (1994) 244–247.
[29] B. Lu, J. Xie, C. Wu, Y. Wei, Anal. Chem. 67 (1995) 83–87.
[30] Y. Jimbo, M. Saito, J. Mol. Electron. 4 (1988) 111–118.
[31] R.A. Hann, in: G. Roberts (Ed.), Langmuir–Blodgett Films, Plenum press, New York, 1990, Chapt. 2.
[32] E. Györvary, W.M. Albers, J. Peltonen, Langmuir 15 (1998) 2516–2524.
[33] I. Vikholm, W.M. Albers, H. Välimäki, H. Helle, Thin Solid Films 327-329 (1998) 643–646.
[34] E. Ishikawa, J. Immunoassay 4 (1983) 209–328.
[35] J. Sadowski, I. Korhonen, J. Peltonen, Opt. Eng. 34 (1995) 2581–2586.
[36] E. Kretschmann, H. Raether, Phys. J. 241 (1968) 313–321.
[37] T. Viitala, W.M. Albers, I. Vikhom, J. Peltonen, Langmuir 14 (1998) 1272–1277.
[38] G. Gorwyn, G.T. Barnes, Langmuir 6 (1990) 222–230.
[39] J. Villalaín, Eur. J. Biochem. 241 (1996) 586–593.
[40] V.R. Sarma, E.W. Silverton, D.R. Davies, W.D. Terry, J. Biol. Chem. 246 (1971) 3753–3759.
[41] J. Buijs, J.W.Th. Lichtenbelt, W. Norde, J. Lyklema, Colloids Surf. B: Biointerf. 5 (1995) 11–23.
[42] F. Höök, M. Rodahl, P. Brzezinski, B. Kasemo, Langmuir 14 (1998) 729–734.
[43] G. Elender, M. Kuhnrer, E. Sackmann, Biosens. Bioelectron. 11 (1996) 565–577.
[44] P.-E. Mazeran, J.-L. Loubet, C. Martelet, A. Theretz, Ultramicroscopy 60 (1995) 33–40.
[45] C.L. Riddiford, B.R. Jennings, Biochim. Biophys. Acta 126 (1966) 171–173.
[46] B. Wälivaara, P. Warketin, I. Lundström, P. Tengvall, J. Colloid. Interf. Sci. 174 (1995) 53–60.